Smart Mater. Struct. 4 (1995) 65–74. Printed in the UK

All-moving active aerodynamic surface research

Ron Barrett
Auburn University, Department of Aerospace Engineering, Auburn, Alabama 36849, USA

Received 24 October 1994, accepted for publication 9 February 1995

Abstract. The structural and aerodynamic characteristics of new class of active flight control surface are presented. This new type of surface uses a symmetric, subsonic aerodynamic shell which is supported at the quarter-chord by a main spar and actively pitched by an adaptive torque-plate. The structural mechanics of the torque-plate and several actuator elements are detailed, including newly invented interdigitated electrode (IDE) and constrained directionally attached piezoelectric (CDAP) elements. Laminated plate models demonstrate that both generate similar deflections with comparable torsional stiffness. An experimental torque-plate specimen constructed from PSI-5A-S2 piezoceramic shows high torsional deflections and stiffness as well as excellent correlation with theory. The constrained torque-plate was integrated into a 12.5 cm span × 5 cm chord adaptive missile fin which was designed for Mach 0.6 flight under standard conditions. The specimen showed static pitch deflections up to ±8.1° and dynamic deflections of ±19° at resonance. The active surface was also wind tunnel tested up to 40 m s^{-1} and demonstrated invariant pitch deflections as a function of airspeed, a steady break frequency of 50 Hz, no flutter, buffet or divergence tendencies and steady lift coefficient changes up to ±0.51.

Nomenclature

A, B, D	extensional, coupling and bending stiffness matrices
C_L	lift coefficient
E_3	through thickness electric field
E_L, E_T	longitudinal and transverse element stiffness
N, M	applied forces and moments
OR	orthotropy ratio = E_L/E_T
t	thickness
ΔT	temperature change
T	thickness ratio = t_s/t_a
α	coefficient of thermal expansion, angle of attack
ϵ_{ij}	ijth laminate strain
κ_{ij}	ijth laminate curvature
Λ_i	ith direction actuator free strains
ν_{ij}	Poisson's ratio
ϕ	airfoil pitch angle

subscripts

a	actuator
b	bond
l	laminate
s	substrate

1. Introduction

Since the early days of aeronautics, flight control systems for aircraft have been steadily evolving towards lower weights and higher efficiencies. Today, most aircraft use electro-mechanical, hydraulic or pneumatic actuators to achieve flight control through aerodynamic surfaces. In very small aircraft and munitions, actuators occupy significant fuselage volume, consume much of the available power and contribute sizably to the total weight of the aircraft. Currently, novel techniques for achieving low mass, low volume, high efficiency flight control are being investigated. One of the most unique approaches to compressed flight control involves integration of adaptive materials and flight control surfaces. The first investigation on active aerodynamic surfaces was conducted by Crawley, Lazarus and Warkentin [1]. They constructed a bending-twist coupled graphite-epoxy plate and actively bent it by using conventionally attached piezoceramic sheets. When the plate was exposed to air-loads, it bent further, which increased the twist and accordingly, the control deflections were effectively magnified through the coupling. This first investigation into active aeroservoelasticity was a direct off-shoot of the work conducted by aeroelasticians like Weisshaar who showed that passive structural deflections could be magnified by aerodynamic loading and used to enhance stability and control of aircraft [2].

Numerous other experiments were conducted on many different types of aerodynamic surfaces, including

0964-1726/95/020065 + 02 $19.50

twist-active rotor blades, aircraft wings and missile fins. Barrett demonstrated that ±0.2° static twist reflections could be generated in rotor blades and that ±0.8° deflections were possible in Froude-scaled aircraft wings [3–5]. Ehlers and Weisshaar took earlier work on adaptive wings and missile fins a step further and showed that aeroelastic tailoring coupled with directionally attached piezoceramic (DAP) elements could be used to generate even higher deflections [6–8]. Further analytical studies were done on rotor blades, including the work of Song and Librescu, which showed that active control of rotor blades could be used for vibration reduction [9]. Similar conclusions were drawn by Chen and Chopra who investigated the experimental aspects of active vibration reduction on a 6 ft diameter bearingless helicopter rotor [10]. They showed that 0.3° peak-to-peak twist deflections could be generated. At the same time, fixed wing applications were being examined in greater detail. Lazarus and Crawley examined the characteristics of active lifting surfaces through shape manipulation. This study compared both theory and experiment to show that relatively small deflections could ultimately be used for vibration control [11]. These small, but significant deflections may be used for some forms of vibration reduction and flutter suppression; however, larger deflections are required for full flight control and reduction of buffet vibrations (in fixed-wing aircraft) and blade-vortex interaction vibrations (in rotary-wing aircraft).

One unique approach to active flight control was put forth by Spangler and Hall who constructed an active, hinged flap powered by a bimorph piezoceramic beam [12]. They successfully demonstrated that large control surface deflections were possible in the low subsonic flight regime. This was one of the first investigations to show deflections of a useful magnitude for flight control. Following this initial invention, a host of technologists, further confirmed the findings and began performing experimental investigations on helicopter rotors. Samak and Chopra showed that it may be feasible to build a helicopter rotor with a trailing-edge flap actuator [13]. Griffin and Hanagud examined flaps constructed with no finite hinges [14]. This approach showed smaller but still significant deflections. Finally, Giurgiutiu, Chaudhry and Rogers compared a number of different approaches and concluded that most active rotorcraft vibration control techniques currently produce small deflections or are limited by increasing airspeed [15].

One approach to flight control that produced very high deflections without sensitivity to airspeed was investigated by Barrett [16–18]. He showed that a piezoceramic DAP torque-plate could be mounted within an aerodynamic shell, stiffened by a quarter-chord main spar in bending and actively twisted up to ±4.5°. The resulting twist deflections were used to pitch the entire aerodynamic shell which significantly manipulated airloads—enough for full flight control of many subsonic missiles and remotely piloted vehicles (RPV). Shiao and Chamis also examined the characteristics of the torque-plate fin using a probabilistic approach [19]. A further study by Barrett showed that the aerodynamic shell could be placed such that the main spar was behind the aerodynamic center. This arrangement lent aeroservoelastic characteristics to the surface and effectively magnified the pitch deflections as a function of airspeed. Unfortunately, this aeroservoelastic coupling eventually lead to divergence at approximately 15% beyond the design point.

These early low subsonic torque-plate designs called for a torsionally weak main spar which would be actively twisted along with the torque plate. This led to a significant problem: as the design airspeed was increased, the necessary structural strength of the main spar grew which, in turn, effectively reduced the twisted deflections because of main spar high torsional stiffness. This paper deals with a new design modification to the original torque-plate configuration which effectively skirts the problem of high main spar torsional stiffness and allows for high control deflections up to a transonic flight.

2. Actuator modeling

2.1. Overview of past torque-plate actuator material research

There are a host of different kinds of actuator materials and arrangements that may be used in a torque-plate type flight control surface. Numerous papers have been written on actuator material type and many have been compared. The basic function of the torque-plate is to provide quick, large twist deflections (for high authority flight control) as a moderate torsional stiffness (for high break frequency and resistance to buffet). Accordingly, there are many different ways of generating twist using magnetostrictive, piezoelectric, and shape memory alloy elements. For aeronautics applications, high actuation frequencies and high efficiencies are generally called for; accordingly, the slow response of SMA actuators are fundamentally incompatible with most flight control requirements. Similarly, magnetostrictive elements were not chosen because they require a magnetic coil for actuation which is extremely heavy, only moderately efficient, and dramatically increases equivalent actuator volume.

The volume requirements of piezoelectric and electrostrictive elements, however, are small along with their power consumption and response time. As a result, technologists have successfully integrated these elements into adaptive lifting surfaces for several years. Crawley, Lazarus and Warkentin [1] were the first to apply isotropic conventionally attached piezoceramic (CAP) actuator elements to the surface of bending-twist and extension-twist coupled graphite-epoxy plates. They showed that twist deflections could be generated by actively extending or bending the laminate. Following this initial investigation, it was discovered that isotropic elements could be artificially given highly orthotropic characteristics through tailoring of the attachment area and element geometry [3, 4]. These DAP elements were

Table 1. In-plane properties of interdigitated electrode and baseline PSI-5A-S2 piezoceramic sheet at 500 V mm^{-1} [23, 24].

	IDE ideal	IDE actual	Control (conventional sheet)
Longitudinal strain, Λ_{11}	423 μstrain	324 μstrain	−211.5 μstrain
Lateral strain, Λ_{22}	−211.5 μstrain	−90.8 μstrain	−211.5 μstrain
Longitudinal stifness, E_L	53 GPa	58 GPa(est.)	61 GPa
Lateral stiffness, E_T	61 GPa	61 GPa (est.)	61 GPa

then applied to both coupled and uncoupled substrates and the deflections were measured. As expected, the DAP elements produced twist deflections that were an order of magnitude higher than the CAP elements [16, 17]. The studies were broadened to include piezoelectric polymers like polyvinylidene fluoride (PVDF) and piezoelectric fiber composites [20–22]. It was shown that DAP torque-plates generate 32% more twist and restrained moment that any of the other type of actuator elements that were compared. Since this early study, however, new actuator arrangements and methods of manufacturing adaptive materials have been discovered.

2.2. Interdigitated electrode (IDE) piezoelectric actuator characteristics

One of the most significant modern advances in the field of adaptive structures was recently made by Hagood, Kindel, Ghandi and Gaudenzi [23]. They discovered a method of dramatically increasing longitudinal piezoceramic plate strain while generating transverse strains in the opposite direction. Using interdigitated surface electrodes, they showed that longitudinal strains could be increased by 53%. This important advance is especially applicable to torque-plate design because the higher the orthotropy in actuation strain, the higher the torsional deflections. With actuator elements constructed of PSI-5A-S2 piezoceramic, element performance was compared to a baseline PSI-5A-S2. The ideal performance of an IDE element can be determined assuming that the electrodes are infinitely thin and completely through the thickness of the actuator. This ideal situation is the limiting case for performance of IDE actuators and is shown in table 1.

The conventional arrangement for IDE elements uses surface-bonded electrodes. Although a small amount of piezoceramic actuator is relatively inactive just below the electrodes, the surface patterning of the electrodes is much more amenable to efficient fabrication than through-thickness electrodes. The arrangement of surface-bonded IDE electrodes is shown in figure 1.

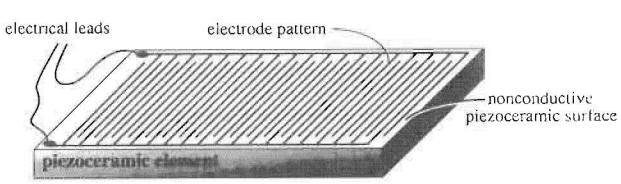

Figure 1. Arrangement of surface-bonded electrodes on an IDE element.

2.3. DAP actuator characteristics

As with the IDE actuators, DAP actuators are also capable of inducing significant shear and twist deflections in laminated structures. However, DAP elements work on a fundamentally different principle. As laid out in [3–5, 16–18], DAP elements can be modeled as generating approximately equal strains in the longitudinal and transverse directions, but they possess significantly different stiffness characteristics. DAP elements are built with conventional piezoceramic sheets, but are attached with specific tailoring so as to significantly reduce the elemental transverse stiffness while maintaining the longitudinal stiffness. When oriented at off-axis angles, these elements may be used to generate shear, twist, bending or extensional motions in coupled or uncoupled lamina. The modeling technique for DAP elements account for three main factors: (i) bond line tailoring, (ii) shear lag, and (iii) end-bond effects. As first explained in [3–5], the effective stiffnesses in the longitudinal and lateral directions are corrected for attachment area. Figure 2 shows a typical attachment schematic for a DAP element using partial attachment.

From figure 2, it is clear that the bond-line patterning alloys for lateral expansion and contraction while maintaining lontigudinal stiffness. In addition to using partial attachment to achieve directional attachment, element geometry and bond thickness also play an important role. Accordingly, directional attachment may also be generated by increasing the aspect ratio of the element. This induces a significant amount of shear lag in the lateral direction which may reduce the effective transverse stiffness, E_{Teff} by as much as 80%. Figure 3 shows how transverse shear lag is used to degrade effective transverse stiffness.

The final form of directional attachment is used mostly to increase orthotropy in the preceeding two and reduce stress risers in the ends of the element. This directional attachment through end-bonding employs stiff bonds on the longitudinal ends of the active element and either no bonds or a very low modulus

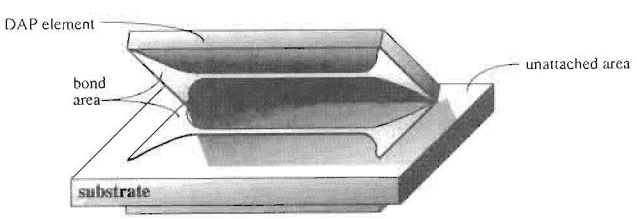

Figure 2. Directional attachment through *partial attachment*.

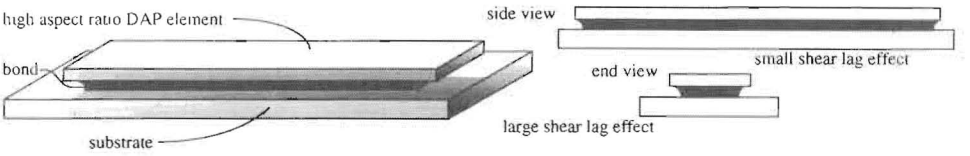

Figure 3. Directional attachment through *transverse shear lag*.

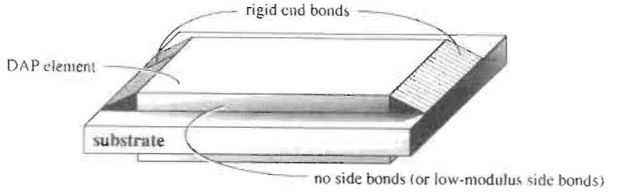

Figure 4. Directional attachment through *differential stiffness bonding*.

bond on the transverse sides of the element. The schematic of this arrangement is shown in figure 4.

In practice, all three methods of achieving directional attachment are used simultaneously to produce the best results. For the generation of twist in adaptive structures, it has been shown that high orthotropy (OR = $E_{\text{Leff}}/E_{\text{Teff}}$) is paramount [16–18]. Early DAP elements operated with orthotropies on the order of 5 to 10 [3–5]. Modern advanced attachment techniques have boosted orthotropies to the 20–50 range. Several prototype elements have even shown OR levels in excess of 100.

For optimum twist generation, it can be seen that both large strain rates and high orthotropy can generate significantly improved twist deflections. Accordingly, table 2 shows the typical and ideal in-plane characteristics along with the properties of a directionally attached interdigitated electrode (DAIDE) actuator element. This DAIDE element would combine the best properties of both actuators.

In addition to providing dramatically improved actuation capability, the directional attachment of the IDE elements would significantly reduce the principal stresses in the active element and increase the lateral strain to failure by several orders of magnitude.

2.3. Theoretical models of DAP, IDE and DAIDE torque-plates

Classical laminated plate theory is a simple and accurate form of analysis for examining the performance of adaptive structures which use piezoceramic sheets. A general equation for an arbitrary laminated plate which is encountering static forces and moments from external sources, piezoelectric actuators and thermal effects can be obtained using the methods outlined by Jones [25].

$$\begin{Bmatrix} N \\ M \end{Bmatrix}_{\text{ex}} + \begin{Bmatrix} N \\ M \end{Bmatrix}_{\text{a}} + \begin{Bmatrix} N \\ M \end{Bmatrix}_{\text{t}} = \begin{bmatrix} A & B \\ B & D \end{bmatrix}_{\text{l}} \begin{Bmatrix} \epsilon \\ \kappa \end{Bmatrix}_{\text{l}}. \quad (1)$$

From past work on adaptive torque-plates it can be seen that isotropic substrates maximize torsional deflections as well as providing the laminate with a high degree of strength in a number of directions [20–22]. Earlier studies also showed that active strains may be maximized by arranging the actuator elements at 45° from the laminate longitudinal axis. By examining the general arrangement of the torque-plate fin, it can also be seen that there are no external forces applied to the laminate, only moments. To manipulate these moments, the elements may be placed either symmetrically or antisymmetrically on the substrate. If the actuator elements were placed antisymmetrically on the laminate and actuated in-phase to provide torsional control, and no bending moments were applied to the laminate, then the laminate would twist and extend in two directions. Assuming that only in-plane extensions from the longitudinal and lateral element directions are used to generate laminate strains and curvatures, then (1) reduces to (2).

$$\begin{Bmatrix} 0 \\ 0 \\ M_{12} \end{Bmatrix}_{\text{ex}} + \begin{bmatrix} A_{11} & A_{12} & 2A_{16} \\ A_{12} & A_{22} & 2A_{26} \\ B_{16} & B_{26} & 2B_{66} \end{bmatrix}_{\text{a}} \times \begin{Bmatrix} \frac{1}{2}(\Lambda_1 + \Lambda_2) + \alpha_{\text{a}}\Delta T \\ \frac{1}{2}(\Lambda_1 + \Lambda_2) + \alpha_{\text{a}}\Delta T \\ \frac{1}{2}(\Lambda_1 - \Lambda_2) \end{Bmatrix} + \begin{bmatrix} (A_{11} + A_{12})_{\text{s}}\alpha_{\text{s}}\Delta T \\ (A_{11} + A_{12})_{\text{s}}\alpha_{\text{s}}\Delta T \\ 0 \end{bmatrix} = \begin{bmatrix} A_{11} & A_{12} & 2B_{16} \\ A_{12} & A_{22} & 2B_{26} \\ B_{16} & B_{26} & 2D_{66} \end{bmatrix}_{\text{l}} \begin{Bmatrix} \epsilon_{11} \\ \epsilon_{22} \\ \kappa_{12} \end{Bmatrix}. \quad (2)$$

Table 2. In-plane properties of typical DAP actuator constructed from PSI-5A-2S piezoceramic sheet at 500 V mm^{-1} [20–22].

	DAP ideal	DAP actual	DAIDE ideal
Longitudinal strain, Λ_{11}	−211 μstrain	−211 μstrain	423 μstrain
Lateral strain, Λ_{22}	−211 μstrain	−211 μstrain	−211 μstrain
Longitudinal stifness, E_{L}	61 GPa	60 GPa	53 GPa
Lateral stiffness, E_{T}	0 GPa	3 GPa	0 GPa

Since the laminate twist, κ_{12}, is directly related to angle of attack of the airfoil shell, the externally applied moment, M_{12}, should be minimized and the thermally induced moment should be eliminated. Clearly, from (2) this cannot be done as the thermally induced strain terms have a large effect on κ_{12}. This is unacceptable as aircraft have widely varying operational temperatures which would inadvertently change the angle of attack. Accordingly, if symmetric elements were used on the torque-plate, then the thermally induced strain terms are not coupled to κ_{12} as can be seen in (3).

$$\begin{Bmatrix} 0 \\ 0 \\ 0 \\ M_{11} \\ M_{22} \\ M_{12} \end{Bmatrix}_{ex} + \begin{bmatrix} A_{11} & A_{12} & 2A_{16} & 0 & 0 & 0 \\ A_{12} & A_{22} & 2A_{26} & 0 & 0 & 0 \\ A_{16} & A_{26} & 2A_{66} & 0 & 0 & 0 \\ 0 & 0 & 0 & B_{11} & B_{12} & 2B_{16} \\ 0 & 0 & 0 & B_{12} & B_{22} & 2B_{26} \\ 0 & 0 & 0 & B_{16} & B_{26} & 2B_{66} \end{bmatrix}_a \times \begin{Bmatrix} \alpha_a \Delta T \\ \alpha_a \Delta T \\ 0 \\ \dfrac{\Lambda_1 + \Lambda_2}{2} \\ \dfrac{\Lambda_1 + \Lambda_2}{2} \\ \dfrac{\Lambda_1 - \Lambda_2}{2} \end{Bmatrix} + \begin{bmatrix} (A_{11} + A_{12})_s \alpha_s \Delta T \\ (A_{11} + A_{12})_s \alpha_s \Delta T \\ 0 \\ 0 \\ 0 \\ 0 \end{bmatrix}$$

$$= \begin{bmatrix} A_{11} & A_{12} & 2A_{16} & B_{11} & B_{12} & 2B_{16} \\ A_{12} & A_{22} & 2A_{26} & B_{12} & B_{22} & 2B_{26} \\ A_{16} & A_{26} & 2A_{66} & B_{16} & B_{26} & 2B_{66} \\ B_{11} & B_{12} & 2B_{16} & D_{11} & D_{12} & 2D_{16} \\ B_{12} & B_{22} & 2B_{26} & D_{12} & D_{22} & 2D_{26} \\ B_{16} & B_{26} & 2B_{66} & D_{16} & D_{26} & 2D_{66} \end{bmatrix}_1 \begin{Bmatrix} \epsilon_{11} \\ \epsilon_{22} \\ \epsilon_{12} \\ \kappa_{11} \\ \kappa_{22} \\ \kappa_{12} \end{Bmatrix}. \tag{3}$$

The reader will notice the presence of applied moments M_{11} and M_{22} in (3) that are not present in (2). This is because the torque-plate fin configuration is constrained from bending by the main spar, root mount and aerodynamic shell. Because the antisymmetric laminate inherently generates no twist when free, no moments are required to counter κ_{11} and κ_{22}. How-ever, the symmetric laminate does indeed generate bending cultures in both directions when free. Accordingly, applied moments, M_{11} and M_{22} are required to force κ_{11} and κ_{22} to nearly zero. If it is assumed that the laminate is constrained completely from bending in both directions and allowed to twist freely, then the laminate twist may be solved for directly:

$$\begin{aligned} \kappa_{12} = {} & (E_L(1 - \nu_{TL})\Lambda_1 - E_T(1 - \nu_{LT})\Lambda_2) \\ & \times ((t_s + 2t_b)t_a + t_a^2)/\{E_s t_s^3(1 - \nu_{LT}\nu_{TL})/6(1 - \nu_s) \\ & + (E_L + E_T - 2E_L\nu_{TL})[(t_2 + 2t_b)^2 t_a/2 \\ & + (t_s + 2t_b)t_a^2 + 2t_a^3/3]\}. \end{aligned} \tag{4}$$

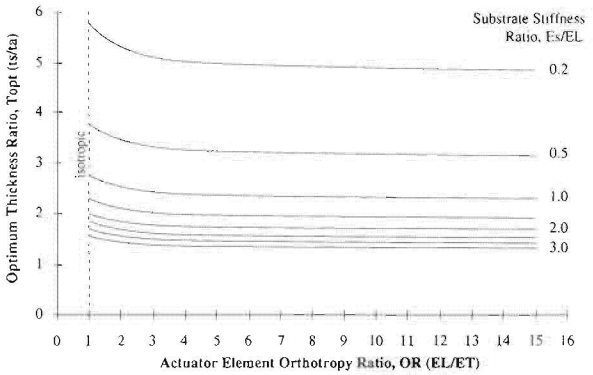

Figure 5. Optimum thickness ratio, T, as a function of orthotropy ratio and substrate stiffness ratio.

Assuming an infinitely thin bond line and casting (4) into a non-dimensional form yields an expression for the non-dimensional laminate twist:

$$\frac{\kappa_{12} t_s}{\Lambda_1} = \frac{\left(\mathrm{OR}(1 - \nu_{TL}) - (1 - \nu_{LT})\dfrac{\Lambda_2}{\Lambda_1}\right)(T^2 + T)}{\dfrac{\mathrm{OR}E_s T^3(1 - \nu_{LT}\nu_{TL})}{6E_L(1 - \nu_s)} + (\mathrm{OR} + 1 - 2\mathrm{OR}\nu_{TL})\left(\dfrac{T^2}{2} + T + \dfrac{2}{3}\right)}. \tag{5}$$

Differentiating (5) with respect to thickness ratio, $T = t_s/t_a$, and setting this expression equal to zero yields an expression for determining the thickness ratio at the maximum non-dimensional laminate twist.

$$T^4 + 2T^3 - \frac{6E_L(1 - \nu_s)(\mathrm{OR} + 1 - 2\mathrm{OR}\nu_{TL})}{\mathrm{OR}E_s T^3(1 - \nu_{LT}\nu_{TL})} \times \left(\frac{T^2}{2} + \frac{4T}{3} + \frac{2}{3}\right) = 0. \tag{6}$$

From (6), it can be seen that the optimum thickness ratio is not a function of actuator strain ratio, Λ_1/Λ_2, but varies chiefly with orthotropy, OR, and substrate stiffness ratio, E_s/E_L as shown in figure 5.

From figure 5, it is clear that the optimum substrate thickness rises as the stiffness is reduced. Also, since IDE elements are approximately isotropic, the optimum substrate thickness will be higher than the substrate thickness for DAP elements which generally have orthotropy ratios from 10–50. A closer examination of torque-plate performance is made assuming an infinitely thin bond line. Figure 6 shows the trends for maximum non-dimensional twist rate as a function of orthotropy ratio, actuator strain ratio, and substrate stiffness ratio.

Using (5), assuming the PSI-5A-S2 elements are attached with an infinitely thin bond to a steel substrate and including the data of tables 1 and 2, a comparison of the twist generation capabilities of DAP, IDE and DAIDE actuators can be made. Figure 7 shows that actual DAP and IDE elements have very similar performance, but IDE elements may ideally generate much higher twist rates.

Figure 7 also shows the DAIDE elements outperform even IDE elements by a significant margin. Accordingly, future torque-plate investigations should include exploration of DAIDE properties.

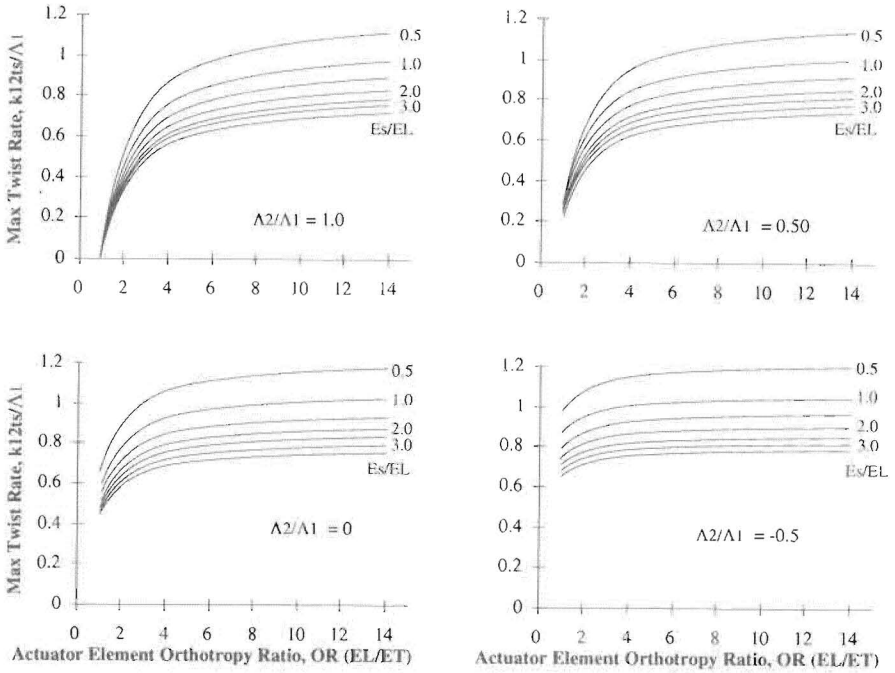

Figure 6. Maximum non-dimensional twist rate, as a function of orthotropy ratio and substrate stiffness ratio.

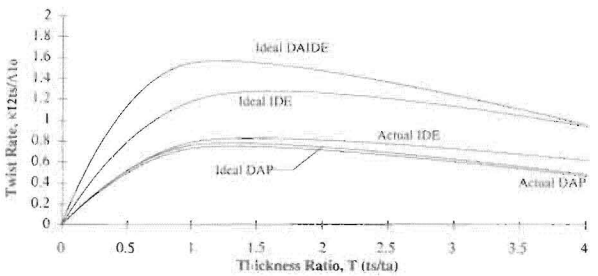

Figure 7. Non-dimensional twist rate for a constrained symmetric torque plate using DAP, IDE and DAIDE elements.

3. Torque-plate design construction and testing

3.1. Design of the torque-plate actuator

The torque-plate was designed to provide high deflections at moderate torsional stiffness levels when constrained from bending longitudinally and laterally. Following the analysis of section 2, the torque-plate was designed to use PSI-5A-S2 piezoceramic sheet actuators. Since highly specialized (and costly) equipment is required to fabricate IDE elements [23], they were not chosen as the torque-plate actuators. Instead, DAP elements were used because they are extremely low cost, require minimal additional fabrication steps, can be rapidly constructed using readily available sand paper and razor blades and provide twist rates that are within 10% of the levels that are currently possible with IDE elements.

The torque-plate dimensions were set at 2.3 cm × 11.0 cm. These were selected to provide the maximum dimensions possible within the shell of a fin which was tailored for a subsonic missile. The piezoceramic was chosen to limit costs; accordingly, 0.1905 mm thick PSI-5A-S2 was used. Through experimental iteration it was discovered that it is extremely advantageous to precompress the piezoceramic elements on any adaptive structure. This is accomplished by choosing a substrate that has a higher coefficient of thermal expansion (CTE) than the piezoceramic and curing at an elevated temperature. Experimentation has shown that steel substrates generally precompress the piezoceramic actuators without initiating compressive failure. This is due to the disparity in CTE between the two materials: $CTE_{steel} = 11\,\mu strain\,^{\circ}C^{-1}$, $CTE_{PSI-5A} = 4\,\mu strain\,^{\circ}C^{-1}$. Using a 120°C cure yields a disparity of 840 μstrain. Other materials have been examined, including aluminum and magnesium. Generally the much higher CTE of these elements are acceptable, but it is impractical (if not impossible) to solder leads to the substrate.

In addition to the use of precompression, other laboratory techniques have been shown to produce good results. Generally, a typical elemental aspect ratio which is high enough to produce large orthotropy, yet low enough to facilitate handling without breakage ranges from 5 to 9. For this study, an aspect ratio of 7 was chosen for manufacturing reasons. From laboratory experience, bond lines of DAP elements can be minimized to 0.05–0.10 mm in thickness. Accordingly, a 0.05 mm thick substrate was chosen, using the techniques described in section 2. The engineering properties of the DAP torque-plate and its constituents are shown in table 3.

3.2. Torque-plate fabrication

The torque plate was fabricated in four main stages. First, the elements were cut and sanded to tolerance;

Table 3. Properties and geometries of DAP torque-plate constraints.

	Material	E_{Leff} (GPa)	E_{Teff} (GPa)	t (mm)
Actuator	PSI-5A-S2	61	3.5	0.191
Substrate	AISI 1010 steel	205	205	0.050
Bond	Scotchweld Adhesive tape	3	3	0.076

second, they were jigged to the proper spacing and angular orientation; third, they were assembled on the substrate and cured; fourth, the torque-plate was de-flashed, leads were surface bonded and a protective coating was added.

The elements were wet cut using a diamond abrasive cutter to 38 mm in length, 5 mm in width in waxed stacks of 20 elements. Bevels of 45° were shaved in the ends of the elements for geometric accommodation and the length was reduced to 33 mm by wet sanding on 400 grit paper. Next, the elements were de-waxed with xylene, de-greased and checked for cracks and dimensional accuracy.

The second stage of assembly involved laying up the elements on a jigging board which aligned the strips to 45° and set their spacing at 0.25 mm. A high-temperature polyester parting tape of 0.025 mm thickness was used to cover up approximately $\frac{2}{3}$ of the element area and to provide a high-aspect ratio bond line. Figures 8 and 9 show the DAP elements during the jigging process.

After jigging, the elements were coated with a 5 mm wide strip of MasterBond conducting epoxy along the centerline of the elements. On either side of the conducting epoxy strip, a pair of strips of Scotchweld adhesive tape were applied. The piezoceramic elements were then laid on top and bottom of the 0.05 mm thick AISI 1010 steel substrate and cured for three hours at 120°C under approximately 2 atmospheres of pressure.

Following removal from the oven, the torque-plate was de-flashed and a 4 mm wide brass electrode was attached to the upper side of the elements using conducting epoxy. Leads were attached to the brass electrode and the substrate and a 0.20 mm thick layer of low modulus epoxy was applied to the entire torque-plate as a protective coating.

3.3. Torque-plate testing

The torque-plate was tested for free and κ_{11}, κ_{22} constrained deflection. After mounting in a seismically stable clamp, the torque-plate was energized with a 1 Hz square wave and the deflections were measured by using a laser beam reflected off the tip of the beam. After free testing, the torque-plate was joined to the main spar and allowed to rotate freely about the main spar centerline. Root and tip constraint was achieved by a rigid bond formed from cyanoacrylate resin. The tip was constrained in bending through attachment to a tip-shim. Figure 10 shows the results of static testing and the prediction of the torque-plate performance using the methods laid out in subsection 3.2 and including the bending stiffness of the brass electrode (which significantly affected the free-plate results).

Figure 10 shows that the free plate experiments slightly outperformed prediction. This may be attributed to errors in properly characterizing the increased bending stiffness of the laminate due to the brass electrodes. The constrained plate performance is over predicted by about 10%. This may be due to incomplete laminate constraint in the transverse direction which slightly relieves actuator element stresses and accordingly reduces twist deflections.

4. Aerodynamic surface design, construction and testing

4.1. Aerodynamic surface design and construction

One of the major innovations contained in this paper is the arrangement of the main spar and torque plate. Both are designed so that bending moments are carried by the

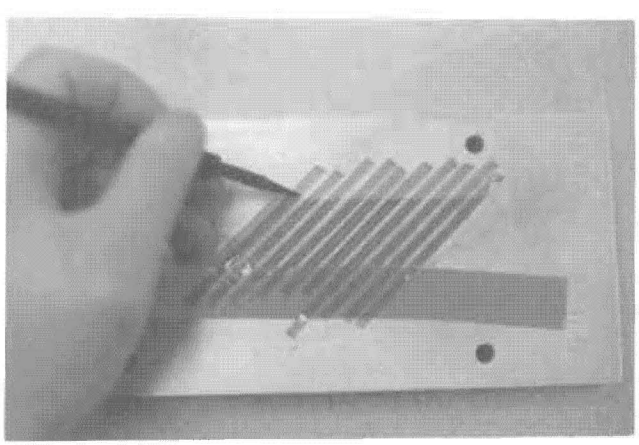

Figure 8. Tape-jigged piezoceramic elements.

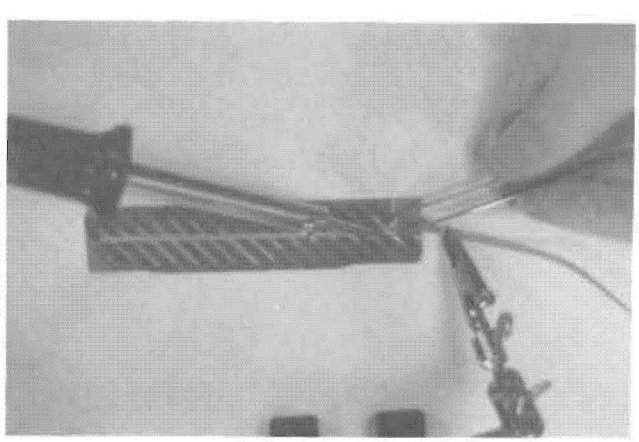

Figure 9. DAP elements bonded to substrate.

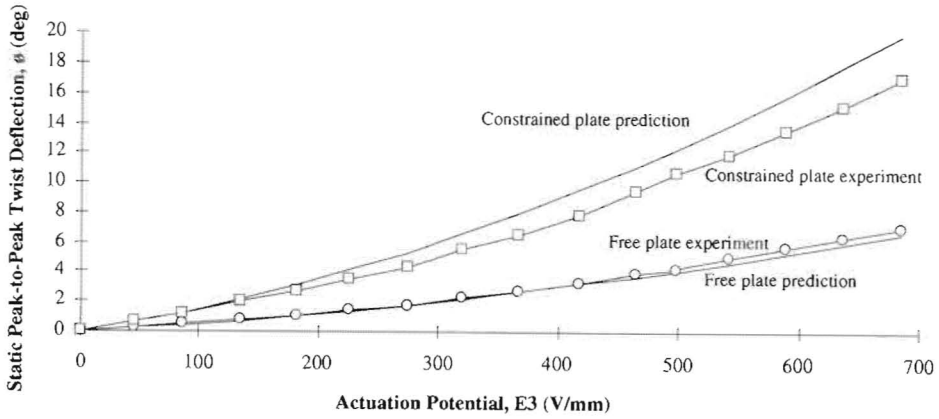

Figure 10. Static peak-to-peak unloaded torque-plate twist deflections.

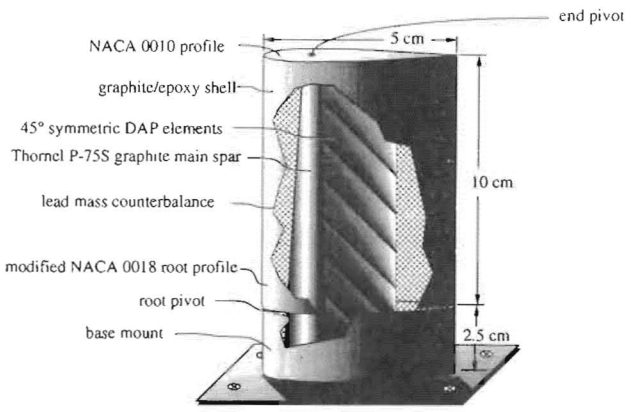

Figure 11. Free-spar aerodynamic flight control surface arrangement.

graphite spar and pitching moments are carried by the torque plate which is torsionally decoupled from the spar. The configuration of this free-spar torque-plate aerodynamic surface is shown in figure 11.

The free-spar aerodynamic surface was designed with semi-span aspect ratio of 2.5 and rectangular planform. The surface was designed to endure loads at $C_{L\max}$, Mach 0.6, standard conditions with a safety factor of 2.0. Using the quasi-vortex lattice method (QVLM) code of [26], the aerodynamic loads were estimated and a graphite spar was designed using the finite element code Cosmos^{TM}. The outer 80% span of the shell was free to pivot about the main spar which accommodated a pair of steel pins, one at the shell root, and one at the tip. The aerodynamic shell was constructed from a graphite/epoxy composite which was cured under pressure at 177°C. A lead counterbalance was integrated into the leading-edge of the airfoil so as to position the center of mass of the airfoil at the quarter chord, which was the location of the aerodynamic center, main spar and hinge line.

4.2. Aerodynamic surface testing

The free-spar torque plate aerodynamic surface was wind-tunnel tested in the low speed $2' \times 3'$ wind tunnel at the University of Kansas. Figure 12 shows the static deflections and accompanying changes in lift coefficient that were generated.

The pitch deflections were measured by reflecting a laser off a conformally mounted mirror which was embedded in the aerodynamic surface. In addition to static testing, the airfoil was excited dynamically at 30 V mm^{-1} from 2 through 54 Hz. The deflections as a function of frequency are shown in figure 13.

Figures 12 and 13 clearly show that from 0 to 40 m s^{-1} the airfoil is relatively insensitive to changes in angle of attack. During testing, the active aerodynamic surface was carefully observed and it showed no flutter or divergence tendencies. The error bars on figure 12

Table 4. Free-spar torque plate flight control surface dimensions and physical characteristics.

Shell mass	23.2 g
Torque-plate mass	8.3 g
Base mount and spare mass	10.7 g
Total free-spar torque-plate flight control surface mass	42.2 g
DAP element dimensions	33 mm × 5 mm
Actuator element type	0.1905 mm PSI-5A-S2 piezoceramic
Actuator arrangement on substrate	45° symmetric
Orthotropy ratio, OR	17.4
Longitudinal stiffness, E_L	61 GPa
Lateral stiffness, E_T	3.5 GPa
Substrate material	0.05 mm AISI 1010 steel foil
Bond material	Scotchweld adhesive tape
Shell and spar material	BASF 5225-W630-500-3K graphite epoxy
Material cost	$83.40

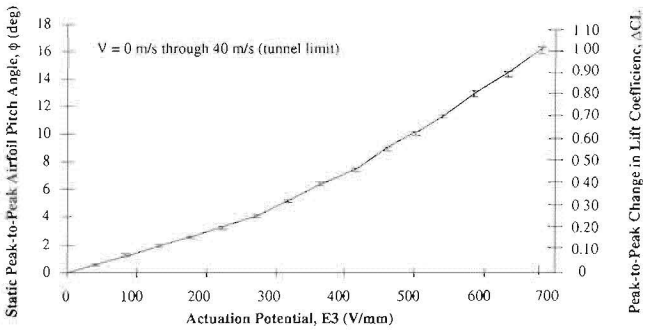

Figure 12. Deflections and lift coefficient changes available from free-spar torque plate aerodynamic surface.

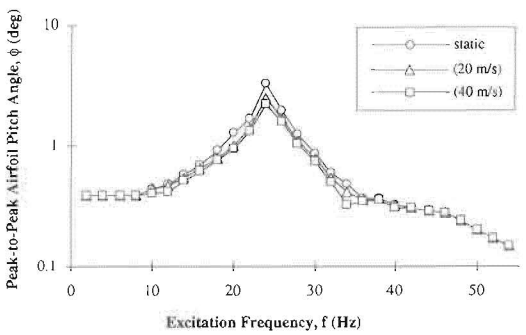

Figure 13. Dynamic airfoil deflections as a function of frequency at 0, 20 and 40 m s^{-1} airspeed.

were due primarily to tunnel turbulence which caused unsteady deflections of approximately ±0.1°. (The turbulence intensity factor was measured at approximately 1.15.) Figure 14 shows the torque-plate aerodynamic surface mounted in the wind tunnel during dynamic testing.

Table 5. Free-spar torque plate flight control surface performance data.

Maximum peak-to-peak active pitch angle change	16.2°
Maximum peak-to-peak lift coefficient change, ΔC_L	1.02
Natural frequency (0 to 40 m s^{-1})	24 Hz
Break frequency	51 Hz

Overall, it can be seen that the feasibility of the free-spar torque-plate fin has been proven for flight speeds up to 40 m s^{-1}. Since the fin is structurally designed to carry loads up to 200 m s^{-1}, the fin is well suited for many types of subsonic flight control applications.

5. Conclusions

It can be concluded that current types of IDE bending-constrained torque-plate actuators generate twist deflections in symmetric torque plates with isotropic substrates that are approximately 10% greater than may be induced by DAP actuators.

Directional attachment of IDE actuator elements may increase bending-constrained torque-plate twist rates by a factor of two over conventional IDE actuator elements.

A free-spar torque-plate missile fin using a bending-constrained torque-plate element with the characteristics shown in table 5, demonstrated very high, stable active pitch deflections, and showed a high resistance to buffet loads and no tendency to flutter or diverge during wind tunnel testing at speeds up to 40 m s^{-1}.

6. Acknowledgments

The author wishes to thank the Auburn University

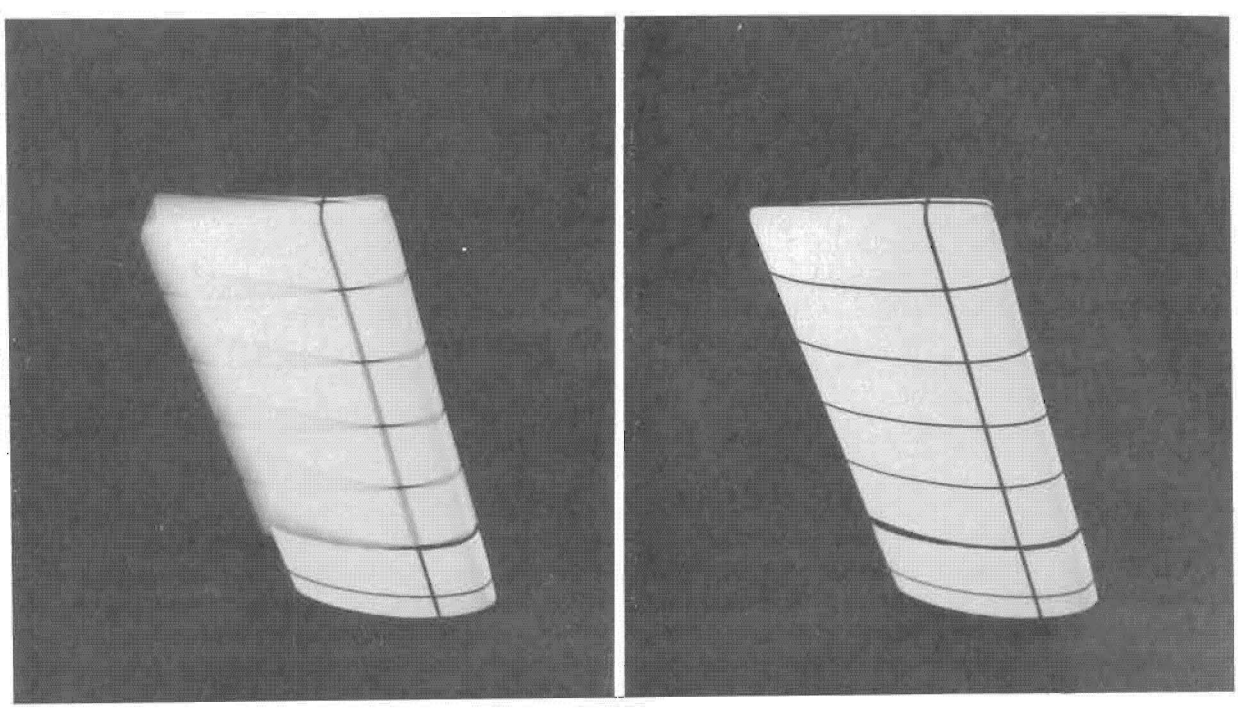

Figure 14. Active and inactive DAP free-spar torque-plate aerodynamic surface undergoing ±6.2° dynamic reflections.

Aerospace Engineering Department for providing laboratory space and supplies and the University of Kansas and NASA Headquarters for partially supporting the research through the Space Grant Consortium. The author also wishes to gratefully acknowledge the support of the US Air Force Armament Directorate for partially supporting this research under contract No FO8630-93-C-0039, Lt. Rob Vickers, program monitor.

References

[1] Crawley EF, Lazarus KB and Warkentin DJ 1989 Embedded Actuation and Processing in Intelligent Materials *2nd Int. Workshop on Comp. Mater. and Structures (Troy, NY, 1989)*

[2] Weisshaar TA 1987 Structural Tailoring for Aircraft Performance *Recent Trends in Aeroelasticity, Structures and Structural Dynamics* Ed P Hajela (Florida: University Press)

[3] Barrett R 1990 Intelligent Rotor Blade and Structures Development Using Directionally Attached Piezoelectric Crystals *MS Thesis* (University of Maryland, MD)

[4] Barrett R 1990 Intelligent Rotor Blade Actuation through Directionally Attached Piezoelectric Crystals *AHS National Forum (Washington, DC)*

[5] Barrett RM Method and Apparatus for Structural Actuation and Sensing in a Desired Direction *US Patent Application 485,599/07*

[6] Ehlers SM and Weisshaar TA 1992 Adaptive Wing Flexural Axis Control *Proc. Third International Conference on Adaptive Structures (San Diego, 1992)*

[7] Ehlers SM and Weisshaar TA 1990 Static Aeroelastic Behavior of an Adaptive Laminated Piezoelectric Composite Wing *AIAA J.* **28** 1611–23

[8] Ehlers SM and Weisshaar TA 1992 Effect of Material Properties on Static Aeroelastic Control *Proc. 33rd SDM Conference (Dallas, TX)*

[9] Song O and Librescu L 1994 Adaptive Vibrational Control of Rotating Helicopter Blades Carrying a Tip Mass *Proc. North American Conference on Smart Materials and Structures (Orlando, Florida)* 52–61.

[10] Chen P and Chopra I 1993 Feasibility Study to Build a Smart Rotor: Induced Strain Actuation of Airfoil Twist *Proc. North American Conference on Smart Materials and Structures (Albuquerque, New Mexico)*

[11] Lazarus KB and Crawley EF 1992 Multivariable Active Lifting Surface Control using Strain Actuation: Analytical and Experimental Results, *Proc. Third International Conference on Adaptive Structures (San Diego)*

[12] Spangler RL and Hall SR 1990 Piezoelectric Actuators for Helicopter Rotor Control *31st Structures, Structural Dynamics and Materials Conference (Long Beach, California)*

[13] Samak DK and Chopra I 1993 Feasibility Study to Build a Smart Rotor: Trailing Edge Flap Actuation *Proc. North American Conference on Smart Materials and Structures (Albuquerque, NM)* 225–37

[14] Griffin S and Hanagud SV 1994 Smart Aerodynamic Control Surface Actuator *Proc. North American Conference on Smart Materials and Structures (Orlando, FL)* 99–106

[15] Giurgiutiu V, Chaudhry Z and Rogers C 1994 Engineering Feasibility of Induced Strain Actuators for Rotor Blade Active Vibration Control *Proc. North American Conference on Smart Materials and Structures (Orlando, Florida)* 107–22

[16] Barrett R 1992 Actuation Strain Decoupling Through Enhanced Directional Attachment in Plates and Aerodynamic Surfaces *Proc. 1st European Conference on Smart Structures and Materials (Glasgow, Scotland)* 383–6

[17] Barrett R 1992 Active plate and wing research using EDAP elements *Mater. Struct.* **1** 214–26

[18] Barrett RM 1994 Active Plate and Missile Wing Development Using DAP Elements *AIAA J.* **32** 601–9

[19] Shiao M and Chamis C 1994 Optimization of Adaptive Intraply Hybrid Fiber Composites with Reliability Considerations *Proc. North American Conference on Smart Materials and Structures (Orlando, Florida)* 484–94

[20] Barrett R 1993 Aeroservoelastic DAP Missile Fin Development *Smart Mater. Struct.* **2** 55–65

[21] Barrett R 1993 Modeling Techniques and Design Principles of a Low Aspect Ratio Active Aeroservoelastic Wing *Proc. North American Conference on Smart Materials and Structures (Albuquerque, New Mexico)* 107–18

[22] Barrett R 1993 Advanced Low-Cost Smart Missile Fin Technology Evaluation, Final report to the United States Air Force, Armament Directorate, Eglin AFB, Florida, Barrett Aerospace Technologies, Lawrence, KS, December, 1993

[23] Hagood NW, Kindel R, Ghandi K and Gaudenzi P 1993 Increasing transverse actuation of electroceramics using interdigitated surface electrodes *Proc. North American Conference on Smart Materials and Structures (Albuquerque, NM)* 341–52

[24] Piezo Systems Product Catalog 1993 *Transducer Elements*, Rev. Piezo Systems Incorporated, Cambridge, Massachusetts

[25] Jones RM 1975 Micromechanical Behavior of a Lamina *Mechanics of Composite Materials* (New York: Hemisphere Publishing Corporation)

[26] Lan CTE 1988 Applied Airfoil and Wing Theory (Taiwan: Cheng Chung Book Company)